Polarization Reconfigurable and Beam-Switchable Array Antenna Using Switchable Feed Network

CHAO LIU[ID], **YONGFENG LI**[ID], **TONGHAO LIU**[ID], **YAJUAN HAN**[ID],
JIAFU WANG[ID], **(Member, IEEE), AND SHAOBO QU**
College of Science, Air Force Engineering University, Xi'an 710051, China

Corresponding authors: Yongfeng Li (liyf217130@126.com) and Shaobo Qu (qushaobo@mail.xjtu.edu.cn)

ABSTRACT A novel array antenna with reconfigurable polarizations and radiation pattern agility is presented in this paper. The digital-controllable array antenna has the functional capabilities of reconfigurable polarization and switching beam, which consists of cavity-backed antenna element based on substrate integrated waveguide (SIW) technique, parasitic patch array, power dividers and phase shifters. Polarization modes and radiation patterns can be dynamically controlled by means of Microcontroller Unit (MCU) with the different feeding ports and phase difference. To validate this proposal, the performance of the fabricated device was measured at the operating frequency of 5.4 GHz. Measured results indicate that the 10 dB impedance bandwidths and 3 dB axial ratio (AR) bandwidths cover from 5.25 to 5.6 GHz, and the measured gains range from 7.9 to 10.1 dBic. The experimentation and simulation verify that the proposed antenna can achieve two polarization states and five radiation beams of each polarization state, which indicate a good performance of the polarization reconfigurable and beam switching antenna array.

INDEX TERMS Polarization reconfigurable, beam switching, reconfigurable feed network, stacked patch structure, substrate integrated waveguide (SIW).

I. INTRODUCTION

With the development of modern wireless communication, reconfigurable antennas based on electrically tunable techniques with its agility to change the operating frequency [6], [16], polarization states [1], [3], [4], and radiation patterns [2], [5] by using PIN diodes [1], [4], [5], MEMS switches [7], varactors [8], [9], dielectric liquid [31] and mechanical rotating [34] have attracted great attentions. Comparing with linearly polarized (LP) antenna, circular polarized (CP) antenna possesses the ability on improving the communication performance [10], eliminating multipath [11] and avoiding polarization mismatch. Among the polarization reconfigurable antennas, beam switchable antenna can be a suitable choice to a variety of different applications, such as internet-of-thing (IoT) and wireless local area networks. These antennas have the advantages of realizing maximize transmit power and avoiding interference of the noise source.

The associate editor coordinating the review of this manuscript and approving it for publication was Giovanni Angiulli[ID].

Recently, many polarization reconfigurable and beam switchable antennas have been proposed for communication, i.e., left-handed circular polarization (LHCP), right-handed circular polarization (RHCP) and linear polarizations (LP). There are three kinds of approaches achieving polarization reconfigurable antenna, the first one is to adopt a reconfigurable feeding network [1], [12], [20]–[22], [25], [30]. [1], [25] is to rebuild the feeding network to excite different LP radiation structure, and the antenna can switch its polarization among LP, LHCP and RHCP. Metamaterials are artificially constructed array structure composed of subwave-length cells and are used as polarization antenna. Using Metamaterials as the radiation patch or reflector, the reconfigurable features can be realized by the reconfigurable feeding network. The antennas in [12], [20], [21], [32] exhibit excellent performance in bandwidth and gain. In [20], a dual-port dual LP mushroom antenna excited by crossed H-shape slot is designed by characteristic mode analysis (CMA), which can realize polarization reconfigurability. By exciting TM_{10} and TM_{20} modes, the mushroom antennas in [32] have realized the broadband

working and boresight radiation. However, the size of Metamaterial antenna [20] is reach to 60*60*3.508 mm^3.

The second solution is to introduce controllable perturbation segments in the antenna's structure [13], [33]. In [13], two switchable shorting vias are adopted in radiation layer for introducing the perturbation, and the LP, RHCP and LHCP modes can be achieved, but the basing circuit and PIN diodes of the radiation layer will distort the radiation pattern of the antenna. Finally, the radiation pattern and polarization reconfigurable antenna can be achieved by using dielectric liquid [3], [31], but the operating features cannot be changed dynamically comparing with PIN diodes and MEMS switches.

Beam switchable antennas [14]–[19] can be realized by antenna structure, phased arrays and the different feeding ports. In [19], a polarization reconfigurable and pattern switchable antenna was achieved by CMA, and the operating feature can be switched by the feeding network. More recently, some digital coding Metamaterial antenna [26] were proposed to dynamically manipulate beams by PIN diodes, and the coding technology is more effective in switching radiation states with low cost and low weight.

For overcoming the difficulty mentioned above and taking advantage of digital coding technology, a CP reconfigurable and beam switchable antenna array is proposed. The operating states can be dynamical controlled by MCU. The remaining text of the paper is organized as follows. In the Section II, the design and operational principle of the proposed antenna is discussed, and then the performance of the antenna element and antenna array is revealed. In the section III, the prototype is fabricated and measured. At the same time the simulated and measured results are presented and analyzed. Finally, the conclusions are provided in the Section IV.

II. ANTENNA CONFIGURATION AND DESIGN

A. ANTENNA ELEMENT AND THE FEEDING NETWORK

The geometry of the proposed polarization reconfigurable antenna element is shown in Fig. 1, and its detail dimensions are illustrated in Table 1. The antenna element consists of three parts, which include the parasitic patch layer, a square substrate integrated waveguide (SIW) cavity layer and the feeding network layer, and all structures are designed on two 0.508-mm and a 0.762-mm thick RO4350B substrates (ε_r = 3.66 and $tan\delta$ = 0.004 at 5.4 GHz). The parasitic patch layer is composed of four-square patches. The square SIW cavity layer includes a circular split ring as a radiation slot and two grounded coplanar waveguide feeding (GCPW) structure [23], [24]. The feeding network layer consists of a polarization switching network, and the parasitic patch layer is introduced for improving the operating frequency band [27], [28].

The square SIW cavity is formed by metallic vias and its length is W_5. The metallic via has the diameter of d and the space between two adjacent metallic vias is p, which
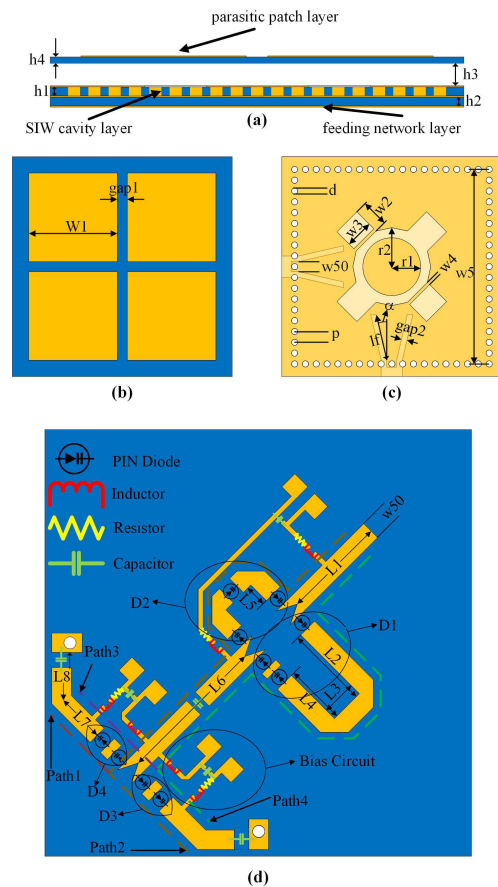

FIGURE 1. Geometrical configuration of the antenna element. (a) Side view. (b) Parasitic patch layer. (c) SIW cavity layer. (d) Feeding network layer.

TABLE 1. Geometrical parameters of the antenna elements.

Parameter	Value	Parameter	Value
h1	0.762	d	1
h2	0.762	p	1.72
h3	1.90	w50	1.60
h4	0.508	w2	5.0
W1	14.1	w3	5.0
gap1	0.6	w4	0.5
gap2	0.9	w5	30.96
r1	4.1	w50	1.60
r2	5.7	L1	9
lf	7.5	L2	6.8
L3	2.9	L4	5
L5	1.8	L6	12.3
L7	3.8	L8	2.3

is designed at operating frequency. The square SIW cavity consists of two switchable feeding ports, GCPW line and annular slot. The GCPW lines are designed to have a 50-ohm characteristic impendence with a width of w_{50}, and a length of lf and a gap of gap_2, which are used to feed the SIW cavity at the port 1 and the port 2. At the same time, the width of 50-ohm input microstrip line is equal to w_{50} for having a smooth transition from microstrip line to GCPW line. A good

return loss can be achieved by tuning the length of *lf* and the deflection angle α of the GCPW line, as shown in Fig. 1(c).

The traditional annular slot radiates linearly polarized waves, when the SIW cavity with annular slot is fed individually by the port1 and port2. It can support two resonating modes, i.e., TE_{210} and TE_{120} modes that similar to a square patch antenna resonating TM_{10} and TM_{01}. To obtain the circular polarization character, two square slots are introduced to generate perturbation and separate two orthogonal modes forming a 90-degree phase difference between the two orthogonal modes. In order to excite the two orthogonal modes, the initial dimension of the square SIW cavity can be calculated by the following formulates [29]:

$$ f_{mnp} = \frac{1}{2\sqrt{\mu\varepsilon}} \sqrt{\left(\frac{m}{L_{eff}}\right)^2 + \left(\frac{n}{W_{eff}}\right)^2 + \left(\frac{p}{h}\right)^2} \quad (1) $$

$$ L_{eff} = W_{eff} = L - 1.08\frac{d^2}{d_p} + 0.1\frac{d^2}{L} \quad (2) $$

where ε and μ are the permittivity and permeability of the substrate. L_{eff} and W_{eff} are the equivalent length and width of the SIW cavity. L is the length of the cavity, $m = 2, n = 1$, $p = 0$. d and d_P are the via diameter and spacing between neighboring vias, respectively. The inner and outer radius of the annular slot can be determined by the formula [30]:

$$ R_1 + R_2 = \frac{c_0}{\pi\sqrt{\varepsilon}f_{mnp}} \quad (3) $$

where c_0 is the velocity of light in free space, and f_{mnp} is the operating frequency. The initial size of the parasitic patches can be determined by the following formula:

$$ w_0 = w_1 = \frac{\lambda_0}{2\sqrt{\varepsilon}} \quad (4) $$

where λ_0 is the wavelength of the operation frequency in free space.

For implementing polarization reconfigurable and beam-switchable, the single-pole double-throw (SPDT) switches are employed to switch polarization states, i.e., LHCP and RHCP, and produce two phase states, i.e., 0 degree and −130 degrees. PIN diodes of four branches are denoted as $D_1 \sim D_4$, as shown in Fig. 1(c). Hence, the polarization and phase states can be considered as two-digital units. The first bit represents the polarization states, i.e., LHCP ('0') and RHCP ('1'), and the second bit represents the phase states, i.e., 0 degree ('0') and −130 degrees ('1'). i.e., '01' are selected, the antenna will radiate LCHP wave with −130 degrees phase when D1 and D4 are ON state, D2 and D3 are OFF state. If '10' are selected, the antenna will radiate RCHP wave with 0 degree phase when D2 and D3 are ON state, D1 and D4 are OFF state (the '00' represents state 1 or Path 1, the '01' represents state 2 or Path 2, the '10' represents state 3 or Path 3 and the '11' represents state 4 or Path 4).

In the implementation, a 2-bit digital programmable antenna element is developed with PIN diodes. Each state has good properties on insertion loss and shift phase difference. In order to get the better insertion loss, the SPDT switch adds
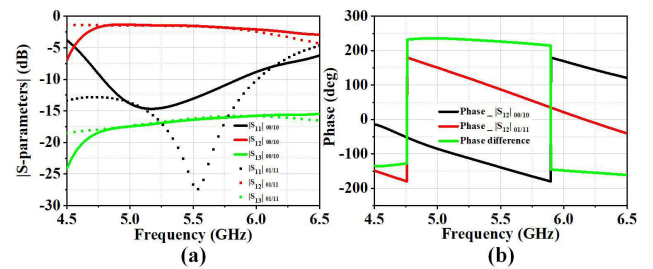

FIGURE 2. Simulated results of the reconfigurable feeding network. (a) Simulated results of the S-parameters. (b) The phase difference.

another PIN diodes in each branch of the SPDT switch. The simulated results are presented in Fig. 2 and demonstrate that the design SPDT switches are capable of switching each state, where the insertion loss of $S12$ and $S13$ represent straight-through port and isolation port.

The Direct Current (DC) bias circuits are introduced to control the PIN diodes (BAR-64L). The Multi-layer Ceramic Capacitors and the Chip inductors with 0402 package are used for DC and Radio Frequency (RF) blocking. The DC power is supplied by the General-purpose input/output (GPIO) of the MCU. The Surface Mounted Devices (SMD) resistors with 0402 package play an important role in limiting the maximum current for matching the drive capability of the GPIO and promise antenna radiation performance. In order to make the feeding structure more compact and improve the effect on radiation performance, polarization switching network, phase shifter and the bias circuits are designed on the feeding network layer as shown in Fig. 1(c).

As a demonstration, the antenna element including DC bias circuits is designed with the help of the full-wave simulator CST, and the final design parametric values are listed in Table 1. As expected, two polarization states are obtained by properly choosing the different excited states of the proposed antenna element, i.e., RHCP state and LHCP state. Fig. 4(a) shows the return loss bandwidth and Axial Radio (AR) bandwidth, where the 10 dB return loss bandwidth are 4.9-5.7 GHz, and the 3dB AR bandwidth are 5.2-5.65 GHz. Fig. 4(b) shows simulated boresight gains with different states polarization of polarization. The simulated radiation patterns at xz-plane and yz-plane are presented in Fig. 4(c) and (d), it can be found that the proposed antenna possesses good far field properties. The surface current distribution of the parasitic patches at different time phases are shown in Fig. 3, which clearly verifies that the antenna operates at CP mode.

B. 2 × 2 ARRAY ANTENNA

Based on the antenna element and the feeding network, a 2 × 2 array antenna with circular polarization-reconfigurable and beam-switchable is developed. In this design, a 4-way power divider which is composed of three 3 dB Wilkinson power dividers is used to feed the different antenna elements. The layout of the array antenna is displayed in Fig. 5.
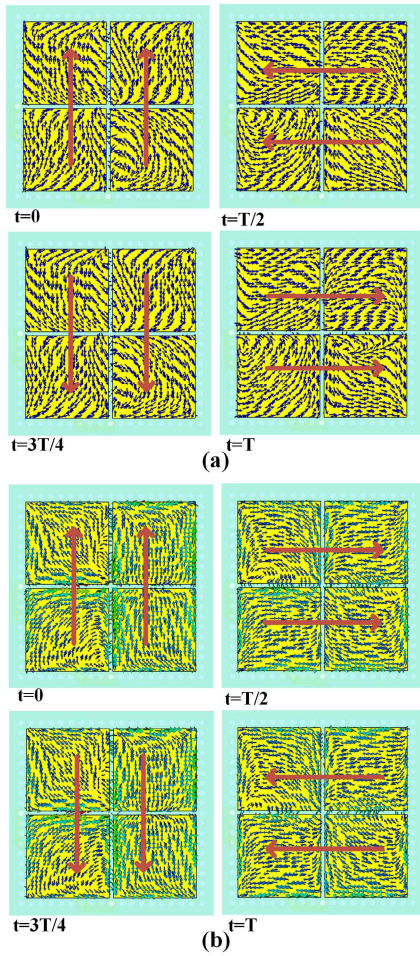
FIGURE 3. Simulated 5.4 GHz surface current distributions at four different time phases. (a) LHCP state. (b) RHCP state.
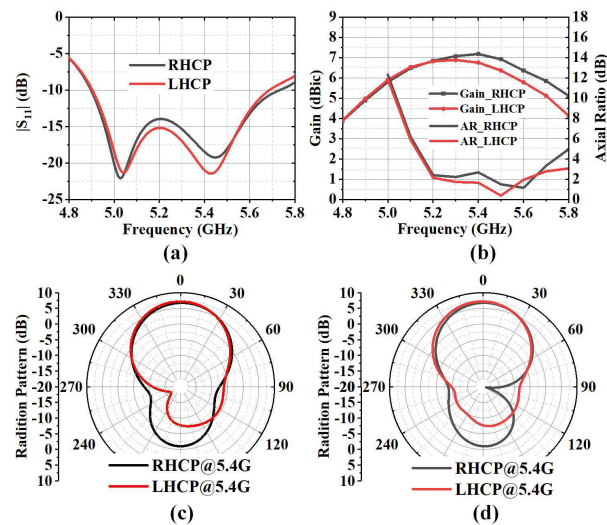

FIGURE 4. The simulated return loss, Axial Radio, boresight gain and the simulated 5.4 GHz radiation patterns of the antenna element. (a) $|s_{11}|$. (b) boresight gain and AR. (c) xz-plane. (d) yz-plane.

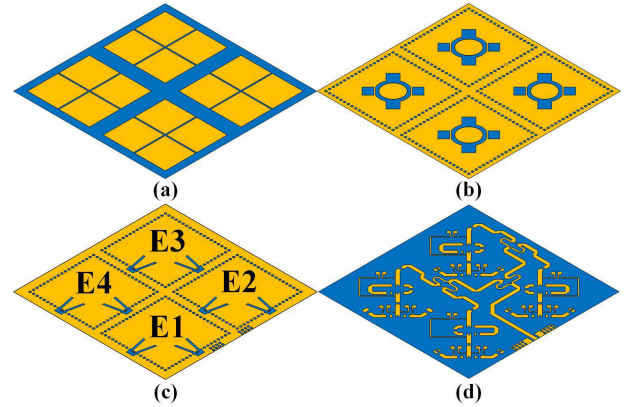The polarization states of antenna element and the radiation beams of the array antenna can be dynamically

FIGURE 5. Layout of the proposed array antenna. (a) Parasitic patch layer view. (b) SIW cavity layer view. (c) Feed port layer view. (d) Feed network layer view.

TABLE 2. Radiation states by different phase.

Polarization States	E1, E2, E3, E4	Coding	Beam	Direction (phi, theta)
0/1	$-130°, -130°,$ $-130°, -130°$	0/1 1111	B1	$0°, 0°$
	$0°, 0°,$ $-130°, -130°$	0/1 0011	B2	$0°, 22°$
	$-130°, -130°,$ $0°, -130°$	0/1 1001	B3	$90°, -22°$
	$-130°, -130°,$ $0°, 0°$	0/1 1100	B4	$0°, -22°$
	$0°, -130°,$ $-130°, 0°$	0/1 0110	B5	$90°, 22°$

controlled by different PIN diodes with different coding sequences of '0' and '1', i.e., LHCP and RHCP, and different phases, i.e., 0 degree and -130 degrees. For example, when all antenna elements operate in LHCP and are fed with -130 degrees, a directional beam (phi = 0, theta = 0) will be produced. The coding sequence is set as '0-1111', where the first bit and the rest of bits represent that all antenna elements operate in LHCP state and phase state of antenna elements E1 $\sim$ E4, respectively, as shown in Fig. 5.

All the radiation states including the corresponding polarization state, phase distribution, coding sequence and the simulated maximum direction are listed in Table 2. In order to clearly observe the radiation states, the simulated far-field 3D radiation patterns of different radiation states are illustrated in Fig. 6 under different coding sequences at LHCP state.

III. EXPERIMENTAL RESULTS

The simulated and measured results of the proposed array antenna under different radiation states are compared and discussed in this section. The prototype has been fabricated by using the low-cost printed circuit board (PCB) technology, and the metals are made of 0.035 mm thick copper layers,
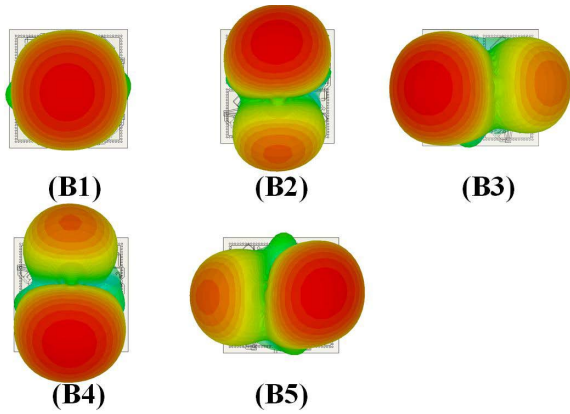
(B1) **(B2)** **(B3)**

(B4) **(B5)**

FIGURE 6. Simulated 5.4 GHz 3D radiation patterns of the proposed array antenna under different coding sequences at LHCP mode.

(a)

(b)

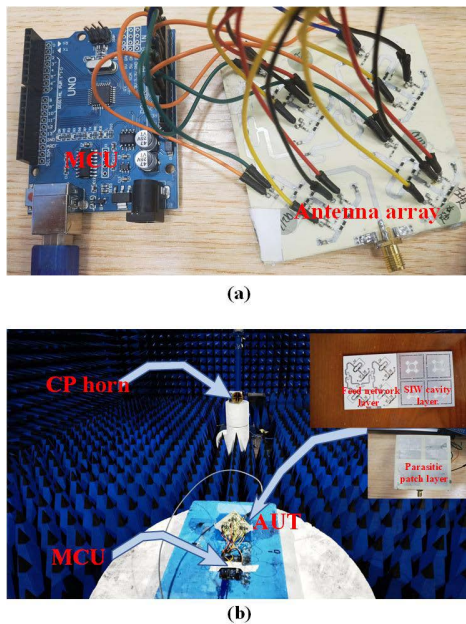**FIGURE 7.** (a) Photograph of the fabricated array antenna prototype. (b) Measurement setup in the anechoic far-field chamber.

(a)

(b)

FIGURE 8. Simulated and measured reflection coefficients of the array antenna at different states. (a) LHCP state. (b) RHCP state.

(a)

(b)

FIGURE 9. Simulated and measured AR properties of the array antenna at different states. (a) LHCP state. (b) RHCP state.

as shown in Fig. 7. A MCU is used to control the radiation states with different coding sequences.

The reflection coefficients of the array antenna were measured under different radiation states by Agilent 8721ET Network Analyzer, and simulated and measured results are plotted in Fig. 8. The measured 10 dB reflection bandwidths are wider than the simulated result for the LHCP, RHCP modes respectively, which are caused by the small tolerance of the fabrication of process and the modeling residue for the actual capacitances that caused by Surface Mounted Technology. At the same time, the simulated resonance point is deviated and another resonant point is introduced.

For measuring the CP properties, circularly polarized horn antenna servers as source antenna. The measured gain and AR of all operating states at the max radiation direction are depicted in Fig. 9 and Fig. 10. The measured gain for
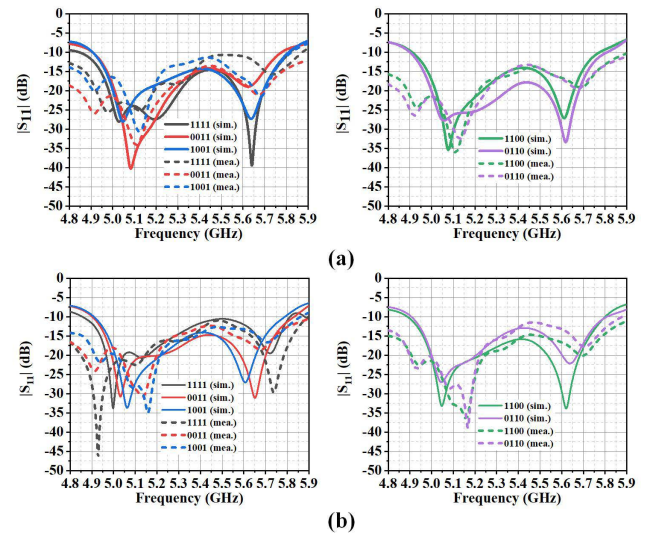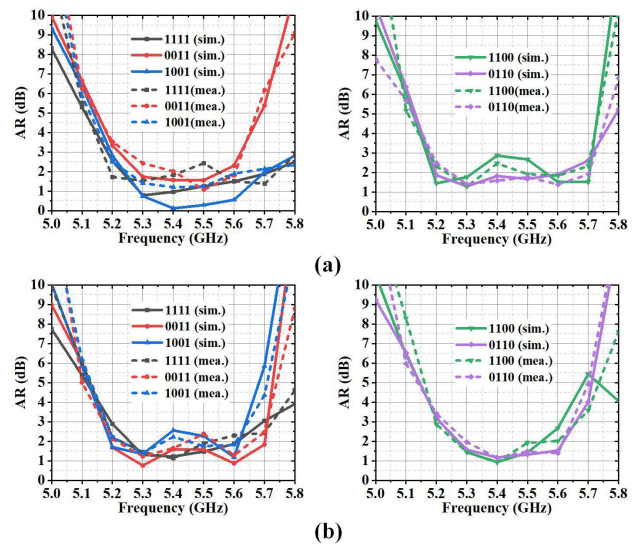
LHCP and RHCP mode range from 7.9 dBic to 10 dBic and 7.8 dBic to 10.1 dBic, respectively, and the measured 3 dB AR bandwidths range from 5.25 to 5.6 GHz for all operating states. It can be observed the measured gains are about 1.4-2 dB smaller than simulated gains, and this discrepancy is caused by the additional loss, i.e., SMA connector, PIN diodes and copper. According to the data sheet of the BAR-64 PIN diode, ON state is equivalent to a 2 ohm resistance, however the actual equivalent circuit model is more complicated which will cause additional heat loss and reduction of the radiation gain. At same time, the substrate, copper, SMA connector and dc bias circuits contribute to corresponding loss which are not taken into consideration in the full-wave simulator. Ignoring errors which caused

TABLE 3. Radiation states by different phase.

Ref	No of Polarization States	Center Frequency (GHz)	Impendence Bandwidth (%)	3 dB AR Bandwidth (%)	Peak Gain (dBi/dBic)	Dimension (mm^3)	No of each polarization beams
[14]	LP	5.7	21	~	19	180*180*3.624	13
[17]	LP	2.4	1.25	~	8.2	100*100*1.5	12
[18]	2CP	2.45	13.1	3.3	11.23	74*74*9.6	1
[19]	2LP 2CP	5	16%	11	4.38(CP) 3.09(LP)	39*39*4	2
[20]	2LP 2CP	5.2	9.74(LP) 38.7(CP)	28	8.73(LP) 8.2(CP)	60*60*3.508	1
[31]	2LP	2.4	22.9	~	4.2	~	1
This work	2CP	5.4	17	6	10.1	74*74*3.932	5

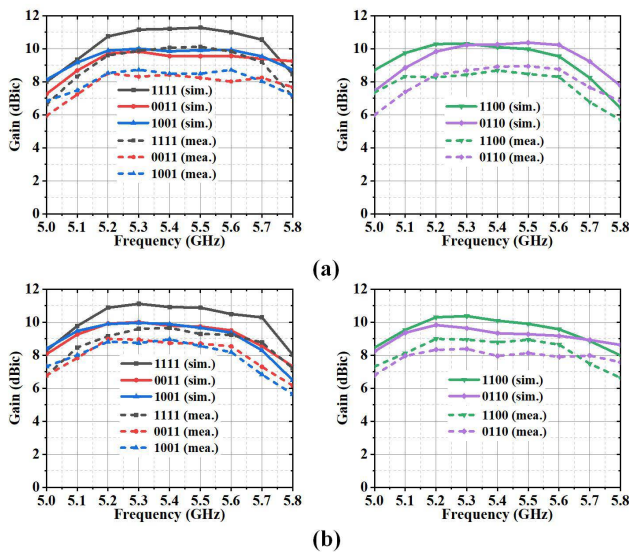**FIGURE 10.** Simulated and measured gain properties of the array antenna at different states. (a) LHCP state. (b) RHCP state.

FIGURE 11. Simulated and measured efficiency for B1 at LHCP state.

by equipment and measurement, the reconfigurable antenna array has stable realized gain over the whole 3 dB AR bandwidth.

To evaluate the measured radiation efficiency of the array antenna, the measured gain and measured radiation efficiency for B1 at LHCP state is depicted in Fig. 11. Due to the symmetry of the array antenna structure, the other operating states have similar result, so the representative operating state, i.e., B1 at LHCP state, is taken into consider for simplicity. The measured radiation efficiency, which is
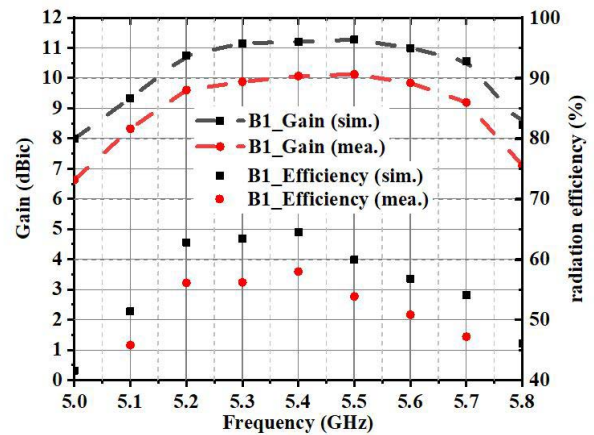
obtained by calculating the ratio of the measured gain to the simulated gain, is about 53% of the entire operating frequency band.

Due to the symmetry array antenna structure, the proposed array antenna possesses similar radiation patterns with different polarization states. As shown in Fig. 12, the measured and simulated normalized radiation patterns with different beams are compared in the LHCP state of 5.4 GHz. The measured results of the radiation patterns have small errors, and the pattern of each state has mild sidelobe. Because the slots of the GCPW feeding lines have serious difference for the measured radiation patterns that bring about the sidelobes deviate the simulated radiation patterns and
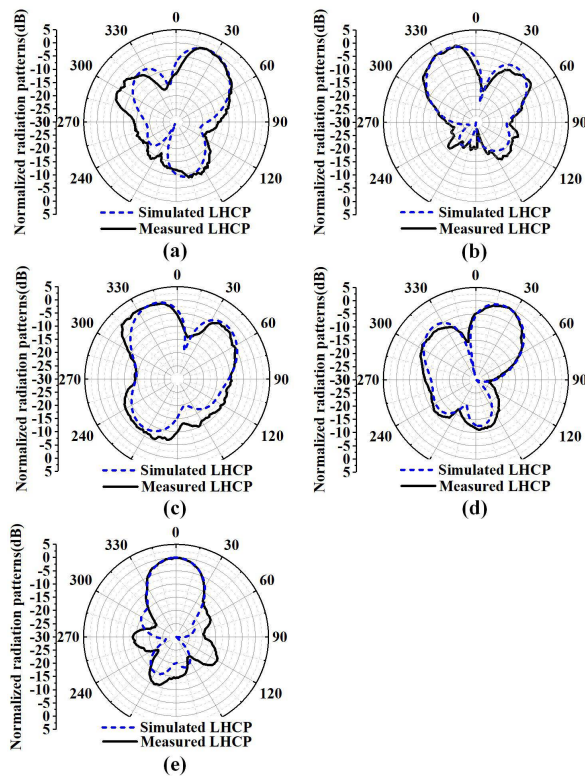
FIGURE 12. Simulated and measured normalized radiation patterns of the array antenna at LHCP state.

larger back-lobe. The dc bias circuit is designed on the bottom layer, which has little effect on the main lobe.

Finally, the performance of some up-to-date polarization reconfigurable antennas and this work are summarized in Table 3 for comparison. From Table 3, it is evident that the proposed reconfigurable array antenna has advantages of wide impendence bandwidth, a high enough gain with two polarization state. At the same time, it has the ability to control the radiation beams by MCU, including B1, B2, B3, B4, B5 radiation beams.

IV. CONCLUSION

To conclude, a polarization reconfigurable array antenna with radiation pattern agility is proposed, which is combined using annular slot antenna element based on SIW technique in this paper. Then the radiation patterns and polarization states can be dynamically altered by different coding sequences using MCU. A prototype of the array antenna is fabricated, debugged and tested under different coding sequences. The measured results are in good agreement with the simulated results considering the various actual errors. The proposed array antenna has the advantages of low-profile structure, the polarization reconfigurable and pattern flexible ability. It can be potentially used for low-cost, polarization reconfigurable antenna in the wireless systems, and this work provides significant guidelines for designing new high-performance reconfigurable antenna.

REFERENCES

[1] X. Ding, Z. Zhao, Y. Yang, Z. Nie, and Q. H. Liu, "A compact unidirectional ultra-wideband circularly polarized antenna based on crossed tapered slot radiation elements," *IEEE Trans. Antennas Propag.*, vol. 66, no. 12, pp. 7353–7358, Dec. 2018, doi: 10.1109/TAP.2018.2867059.

[2] J.-S. Row and L.-K. Kuo, "Pattern-reconfigurable array based on a circularly polarized antenna with broadband operation and high front-to-back ratio," *IEEE Trans. Antennas Propag.*, vol. 68, no. 5, pp. 4109–4113, May 2020, doi: 10.1109/TAP.2019.2948679.

[3] Z. Hu, S. Wang, Z. Shen, and W. Wu, "Broadband polarization-reconfigurable water spiral antenna of low profile," *IEEE Antennas Wireless Propag. Lett.*, vol. 16, pp. 1377–1380, 2017, doi: 10.1109/LAWP.2016.2636923.

[4] L. Zhang, Y. Sun, Y. He, S.-W. Wong, C. Mao, L. Ge, and S. Gao, "A quad-polarization reconfigurable antenna with suppressed cross polarization based on characteristic mode theory," *IEEE Trans. Antennas Propag.*, vol. 69, no. 2, pp. 636–647, Feb. 2021, doi: 10.1109/TAP.2020.3016384.

[5] Y. Liu, W. Zhang, Y. Jia, and A. Wu, "Low RCS antenna array with reconfigurable scattering patterns based on digital antenna units," *IEEE Trans. Antennas Propag.*, vol. 69, no. 1, pp. 572–577, Jan. 2021, doi: 10.1109/TAP.2020.3004993.

[6] H. L. Zhu, X. H. Liu, S. W. Cheung, and T. I. Yuk, "Frequency-reconfigurable antenna using metasurface," *IEEE Trans. Antennas Propag.*, vol. 62, no. 1, pp. 80–85, Jan. 2014, doi: 10.1109/TAP.2013.2288112.

[7] J. M. Kovitz, H. Rajagopalan, and Y. Rahmat-Samii, "Design and implementation of broadband MEMS RHCP/LHCP reconfigurable arrays using rotated E-shaped patch elements," *IEEE Trans. Antennas Propag.*, vol. 63, no. 6, pp. 2497–2507, Jun. 2015.

[8] S. Xiao, C. Zheng, M. Li, J. Xiong, and B.-Z. Wang, "Varactor-loaded pattern reconfigurable array for wide-angle scanning with low gain fluctuation," *IEEE Trans. Antennas Propag.*, vol. 63, no. 5, pp. 2364–2369, May 2015.

[9] M. W. Young, S. Yong, and J. T. Bernhard, "A miniaturized frequency reconfigurable antenna with single bias, dual varactor tuning," *IEEE Trans. Antennas Propag.*, vol. 63, no. 3, pp. 946–951, Mar. 2015.

[10] S. Gao, A. Sambell, and S. S. Zhong, "Polarization-agile antennas," *IEEE Antennas Propag. Mag.*, vol. 48, no. 3, pp. 28–37, Jun. 2006.

[11] J. F. Valenzuela-Valdes, M. A. Garcia-Fernandez, A. M. Martinez-Gonzalez, and D. Sanchez-Hernandez, "The role of polarization diversity for MIMO systems under Rayleigh-fading environments," *IEEE Antennas Wireless Propag. Lett.*, vol. 5, pp. 534–536, 2006.

[12] J. Hu, G. Q. Luo, and Z.-C. Hao, "A wideband quad-polarization reconfigurable metasurface antenna," *IEEE Access*, vol. 6, pp. 6130–6137, 2018, doi: 10.1109/ACCESS.2017.2766231.

[13] J. Hu, Z. C. Hao, and Z. W. Miao, "Design and implementation of a planar polarization-reconfigurable antenna," *IEEE Antennas Wireless Propag. Lett.*, vol. 16, pp. 1557–1560, 2017, doi: 10.1109/LAWP.2017.2650961.

[14] J. Hu, Z.-C. Hao, and Y. Wang, "A wideband array antenna with 1-bit digital-controllable radiation beams," *IEEE Access*, vol. 6, pp. 10858–10866, 2018, doi: 10.1109/ACCESS.2018.2801940.

[15] G. Jin, M. Li, L. Dan, and G. Zeng, "A simple planar pattern-reconfigurable antenna based on arc dipoles," *IEEE Antennas Wireless Propag. Lett.*, vol. 17, no. 9, pp. 1664–1668, Sep. 2018, doi: 10.1109/LAWP.2018.2862624.

[16] A. Ghaffar, X. J. Li, N. Hussain, and W. A. Awan, "Flexible frequency and radiation pattern reconfigurable antenna for multi-band applications," in *Proc. 4th Austral. Microw. Symp. (AMS)*, Feb. 2020, pp. 1–2, doi: 10.1109/AMS48904.2020.9059296.

[17] A. Pal, A. Mehta, D. Mirshekar-Syahkal, and H. Nakano, "A twelve-beam steering low-profile patch antenna with shorting vias for vehicular applications," *IEEE Trans. Antennas Propag.*, vol. 65, no. 8, pp. 3905–3912, Aug. 2017, doi: 10.1109/TAP.2017.2715367.

[18] H. Sun, X. Ge, W. He, and L. Zhao, "A reconfigurable antenna with sum and difference patterns for WLAN access points," *IEEE Antennas Wireless Propag. Lett.*, vol. 19, no. 7, pp. 1073–1077, Jul. 2020, doi: 10.1109/LAWP.2020.2988690.

[19] W. Li, Y. M. Wang, Y. Hei, B. Li, and X. Shi, "A compact low-profile reconfigurable metasurface antenna with polarization and pattern diversities," *IEEE Antennas Wireless Propag. Lett.*, vol. 20, no. 7, pp. 1170–1174, Jul. 2021, doi: 10.1109/LAWP.2021.3074639.

[20] P. Liu, W. Jiang, S. Sun, Y. Xi, and S. Gong, "Broadband and low-profile penta-polarization reconfigurable metamaterial antenna," *IEEE Access*, vol. 8, pp. 21823–21831, 2020, doi: 10.1109/ACCESS.2020.2969488.

[21] Z. Wu, H. Liu, and L. Li, "Metasurface-inspired low profile polarization reconfigurable antenna with simple DC controlling circuit," *IEEE Access*, vol. 7, pp. 45073–45079, 2019, doi: 10.1109/ACCESS.2019.2908928.

[22] N. Zhu, X.-X. Yang, T. Lou, Q. Cao, and S. Gao, "Broadband polarization-reconfigurable slot antenna and array with compact feed network," *IEEE Antennas Wireless Propag. Lett.*, vol. 18, no. 6, pp. 1293–1297, Jun. 2019, doi: 10.1109/LAWP.2019.2915650.

[23] R. Kazemi, A. E. Fathy, S. Yang, and R. A. Sadeghzadeh, "Development of an ultra wide band GCPW to SIW transition," in *Proc. IEEE Radio Wireless Symp.*, Jan. 2012, pp. 171–174, doi: 10.1109/RWS.2012.6175308.

[24] S. K. Sahoo, M. Adhikary, A. Biswas, and M. J. Akhtar, "GCPW to SIW transition for planar excitation of Ku-band substrate integrated end-fire antennas," in *Proc. IEEE Indian Conf. Antennas Propogation (InCAP)*, Dec. 2019, pp. 1–4, doi: 10.1109/InCAP47789.2019.9134585.

[25] X. Ding, Z. Zhao, Y. Yang, Z. Nie, and Q. H. Liu, "Wideband quad-polarization reconfigurable antenna using switchable feed network with stable unidirectional radiation patterns," *IEEE Access*, vol. 6, pp. 73434–73443, 2018, doi: 10.1109/ACCESS.2018.2884232.

[26] C. Huang, B. Sun, W. Pan, J. Cui, X. Wu, and X. Luo, "Dynamical beam manipulation based on 2-bit digitally-controlled coding metasurface," *Sci. Rep.*, vol. 7, p. 42302, Feb. 2017.

[27] F. Zhang, F.-S. Zhang, C. Lin, and G. Zhao, "Broadband microstrip patch antenna array using stacked structure," in *Proc. Int. Conf. Microw. Millim. Wave Technol.*, Chengdu, China, May 2010, pp. 388–391.

[28] W. Yang, J. Zhou, Z. Yu, and L. Li, "Single-fed low profile broadband circularly polarized stacked patch antenna," *IEEE Trans. Antenna Propag.*, vol. 62, no. 10, pp. 5406–5410, Oct. 2014.

[29] Z. C. Hao, X. Liu, X. Huo, and K. K. Fan, "Planar high-gain circularly polarized element antenna for array applications," *IEEE Trans. Antennas Propag.*, vol. 63, no. 5, pp. 1937–1948, May 2015.

[30] K.-L. Wong, C.-C. Huang, and W.-S. Chen, "Printed ring slot antenna for circular polarization," *IEEE Trans. Antennas Propag.*, vol. 50, no. 1, pp. 75–77, Jan. 2002, doi: 10.1109/8.992564.

[31] J. Ren, Z. Zhou, Z. H. Wei, H. M. Ren, Z. Chen, Y. Liu, and Y. Z. Yin, "Radiation pattern and polarization reconfigurable antenna using dielectric liquid," *IEEE Trans. Antennas Propag.*, vol. 68, no. 12, pp. 8174–8179, Dec. 2020, doi: 10.1109/TAP.2020.2996811.

[32] Q. Chen, H. Zhang, Y.-J. Shao, and T. Zhong, "Bandwidth and gain improvement of an L-shaped slot antenna with metamaterial loading," *IEEE Antennas Wireless Propag. Lett.*, vol. 17, no. 8, pp. 1411–1415, Aug. 2018, doi: 10.1109/LAWP.2018.2848639.

[33] S. W. Lee and Y. J. Sung, "Simple polarization-reconfigurable antenna with T-shaped feed," *IEEE Antennas Wireless Propag. Lett.*, vol. 15, pp. 114–117, 2016, doi: 10.1109/LAWP.2015.2432462.

[34] L. Li, Y. Li, Z. Wu, F. Huo, Y. Zhang, and C. Zhao, "Novel polarization-reconfigurable converter based on multilayer frequency-selective surfaces," *Proc. IEEE*, vol. 103, no. 7, pp. 1057–1070, Jul. 2015, doi: 10.1109/JPROC.2015.2437611.

CHAO LIU is currently pursuing the M.S. degree in physical electronics with Air Force Engineering University, Xi'an, Shanxi, China. His research interests include metasurfaces and antennas design.

YONGFENG LI received the B.S., M.S., and Ph.D. degrees in physical electronics from Air Force Engineering University, Xi'an, Shanxi, China, in 2008, 2010, and 2015, respectively. He has been with Air Force Engineering University, since 2015. His research interests include the surface wave, phase gradient metasurfaces, code metasurfaces, and spoof surface plasmon polaritons.
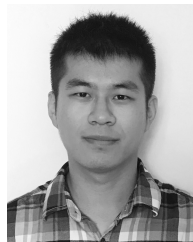
TONGHAO LIU received the B.S. degree in aircraft dynamic engineering from Air Force Engineering University, Xi'an, Shaanxi, China, in 2018, where he is currently pursuing the doctor's degree in electronic science and technology. His research interests include the design of metasurface, surface waves, and surface plasmon polaritons.

YAJUAN HAN received the B.E. degree in electrical engineering and automation from the Hefei University of Technology, Hefei, Anhui, China, in 2012, the M.S. degree in electronic science and technique from Air Force Engineering University, Xi'an, China, in 2017, and the Ph.D. degree from the School of Physics and Optoelectronic Engineering, Xidian University. Her research interests include metasurfaces, spoof surface plasmon polaritons, and antenna design based on metasurface, and spoof surface plasmon polaritons.

JIAFU WANG (Member, IEEE) received the B.S. degree in radar engineering, the M.S. degree in optics engineering, and the Ph.D. degree in physical electronics from Air Force Engineering University, Xi'an, Shanxi, China, in 2004, 2007, and 2010, respectively. He has been with Air Force Engineering University, since 2011, where he is currently an Associate Professor in physical electronics. His current research interests include plasma stealth, design of metamaterials, and application of the metamaterials in microwave.

SHAOBO QU received the B.S. degree in physics from the Fuyang Normal College, Fuyang, Anhui, China, in 1984, the M.S. degree in physics from Sichuan Normal University, Chengdu, China, in 1991, and the Ph.D. degree in materials science and engineering from Northwest Polytechnical University, Xi'an, China, in 2001. Since 2001, he has been with the Department of Applied Mathematics and Physics, Air Force Engineering University, Xi'an, where he is currently a Professor in physical electronics. His research interests include materials physics, metamaterials, electronic materials, and devices.

• • •